Time-dependent traction force microscopy for cancer cells as a measure of invasiveness

Valentina Peschetola, Valérie M. Laurent, Alain Duperray, Richard Michel, Davide Ambrosi, Luigi Preziosi, Claude Verdier

Time–dependent traction force microscopy for cancer cells as a measure of invasiveness

Valentina Peschetola[1,5], Valérie M. Laurent[1], Alain Duperray[2,3], Richard Michel[1]
Davide Ambrosi[4], Luigi Preziosi[5], Claude Verdier[1*]

(1) CNRS / Univ. Grenoble 1, LIPhy UMR 5588, Grenoble, F-38041, France
(2) INSERM U823, Grenoble, France
(3) Univ. Grenoble 1, Faculté de Médecine, Institut d'oncologie/développement, Albert Bonniot et Institut Français du Sang, UMR-S823, Grenoble, France
(4) MOX - Dipartimento di Matematica, Politecnico di Milano, Piazza Leonardo da Vinci 32, 20131 Milano, Italy
(5) Department of Mathematics Politecnico di Torino, Corso Duca degli Abruzzi 24, 10129 Torino, Italy

Abstract

The migration of tumor cells of different degrees of invasivity is studied, on the basis of the traction forces exerted in time on soft substrates (Young modulus $\sim 10kPa$). It is found that the outliers of the traction stresses can be an effective indicator to distinguish cancer cell lines of different invasiveness. Here we test two different epithelial bladder cancer cell lines, one invasive (T24), and a less invasive one (RT112). Invasive cancer cells move in a nearly periodic motion, with peaks in velocity corresponding to higher traction forces exerted on the substrate, whereas less invasive cells develop traction stresses almost constant in time. The dynamics of focal adhesions as well as cytoskeleton features reveals that different mechanisms are activated to migrate: T24 cells show an interconnected cytoskeleton linked to mature adhesion sites, leading to small traction stresses, whereas less invasive cells (RT112) show a less–structured cytoskeleton and unmature adhesions corresponding to higher traction stresses. Migration velocities are smaller in the case of less invasive cells. The MSD (Mean Squared Displacement) shows super–diffusive motion in both cases with higher exponent for the more invasive cancer cells.

Further correlations between traction forces and the actin cytoskeleton reveal an unexpected pattern of a large actin rim at the RT112 cell edge where higher forces are colocalized, whereas a more usual cytoskeleton structure with stress fibers and focal adhesions are found for T24 cancer cells. We conjecture that this kind of analysis can be useful to classify cancer cell invasiveness.

Keywords : cancer cells, traction forces, invasiveness, adhesion, migration, MSD.

*Corresponding author, claude.verdier@ujf-grenoble.fr

Introduction

Cell migration has been studied since many years and it is well known that the shape of cells during motion obeys to multiscale processes (in time and space) [Keren et al., 2008]. The basic mechanism is the cytoskeleton remodelling driven by the actin machinery [Pollard and Borisy, 2003], balanced by the traction forces exerted on the substrate [Balaban et al., 2001; Dembo and Wang, 1999; Fournier et al., 2010]. These seem to correlate with the development of focal complexes [Balaban et al., 2001; Galbraith et al., 2002; Giannone et al., 2007]. The cell velocity of migration is therefore connected with its ability to form/break bonds on substrates and contract its own body to move forward. But it has also been shown [Gupton and Waterman-Storer, 2006] that rapid migration does not necessarily correspond to an organized system between actin, myosin II and focal adhesions (FAs).

Although the arrival of new microscopy techniques [Friedl et al., 2001; Iordan et al., 2010] makes it possible to determine traction forces in three dimensions [Maskarinec et al., 2009; Legant et al., 2010; Delanoë-Ayari et al., 2010], most studies have focused on cells adhering on plane polymeric substrates. PA (PolyAcrylamide) substrates properly coated with Extra–Cellular Matrix (ECM) components such as fibronectin or collagen are an effective adhesion surface.

Traction force methods couple inversion methods and microscopy in order to reconstruct the local values of forces/displacements developed by cells. Most methods use fluorescent beads embedded in PA substrates, and correlation techniques to reconstruct the displacement field. All methods need a regularization (usually the Tikhonov penalization) and adequate filtering of the data. Four main techniques are currently available: Traction Reconstruction with Point Forces (TRPF) [Schwarz et al., 2002], Fourier Transform Traction Cytometry (FTTC) [Butler et al., 2002], the classical Boundary Element Method (BEM) [Dembo and Wang, 1999] and the more recent Adjoint Method (AM) [Ambrosi, 2006; Ambrosi et al., 2009]. A recent work [Sabass et al., 2008] gives a comparison between the first three methods and explains how to improve them by adequate filtering and regularization. Similarly, improvements in the resolution are also available by comparing FTTC and TRPF methods [Stricker et al., 2010], or FTTC and AM [Michel et al., 2012]. Earlier methods use wrinkled patterns on soft PDMS [Harris et al., 1980; Burton and Taylor, 1997] or the deformation of microposts [Tan et al., 2003]. However, wrinkled patterns do not provide traction maps or are difficult to analyze, while microposts use a direct method but provide a non–continuous environment, so we will rather focus here on the previous 2D methods on soft substrates, and the AM method in particular.

Several authors studied the role of substrate rigidity [Lo et al., 2000; Discher et al., 2005;

Ghibaudo et al., 2008; Ambrosi et al., 2009], substrate anisotropy [Saez et al., 2007] and topography [Ghibaudo et al., 2009], as well as the effect of ECM protein density [Palecek et al., 1997] on cell migration. Cells are known to migrate more efficiently on rigid substrates [Lo et al., 2000], although this phenomenon is cell–dependent [Discher et al., 2005], and the velocity of migration seems to find an optimum for a specific matrix protein concentration [Palecek et al., 1997]. This behavior is related to stiffening of the integrin–cytoskeleton bonds [Choquet et al., 1997] with matrix rigidity. Focal adhesions are indeed connected through integrin bounds, their size being proportional to the applied forces [Balaban et al., 2001]. Nevertheless, it seems that this linear relation is only valid at short times [Stricker et al., 2011] when myosin–mediated contractions and focal maturation are at work, and that long term adhesion (with mature adhesions) does not exhibit this correlation.

Although these methods are quite promising and provide adequate tools for linking forces with cytoskeleton and focal complexes, more research is still needed to understand the precise mechanisms by which cells migrate in time. In particular, few studies involve cancer cells on 2D–substrates or lead to contradictory results [Mierke et al., 2008; Indra et al., 2011; Kraning-Rush et al., 2012]. It is therefore interesting to determine *in vitro* methods for comparing quantitatively migration speed, applied forces, to the possibly correlated fluorescence images of the cytoskeleton and focal complexes in time. It is indeed possible that cancer cells develop particular forces and specific adhesion mechanisms to propel themselves through tissues or to extravasate. Such observations were initially proposed [Munevar et al., 2001] by comparing fibroblasts with H-ras transformed fibroblast (known to exhibit mestastatic potential after injection of the H-ras oncogene [Bondy et al., 1985]). The latter ones showed smaller traction forces, and a disorganized motile behavior. Recently other researchers [Indra et al., 2011] found inverse correlation between traction forces/adhesion strength and the metastatic potential of different cancer cells, but on the other hand another recent work reports opposite results [Kraning-Rush et al., 2012].

Here we provide a detailed analysis of the time–dependent behavior for two cancer cell lines (T24 and RT112, which are epithelial bladder cell lines) and measure the traction forces exerted on PA substrates coated with collagen. These features are correlated with data from complementary migration assays of migration velocities, while fluorescence microscopy enables us to quantify the cytoskeleton changes as well as focal adhesions. Finally traction force locations are investigated in relation with the actin dynamics. Section 2 presents the materials and methods used in this work. In section 3, the main results are illustrated concerning traction forces, immunofluorescence and migration velocities. Finally, results are compared and discussed in section 4.

Materials and methods

Cell culture

Epithelial bladder cancer cell lines used in this study were obtained from ATTC (Rockville, USA) and were cultured in RPMI 1640 (Sigma Chemical Co.) supplemented with 10% fetal bovine serum and antibiotics. Cultures were kept at 37 °C in 5% CO_2 humidified atmosphere. In particular, two bladder carcinoma cell lines have been investigated: T24 and RT112. T24 cancer cells are poorly differentiated and have a cytological grade 3. The RT112 line is a moderately differentiated one and is characterized by cytological grade 2. *In vitro*, T24 cells display a high invasive capacity, whereas RT112 cells present a moderate invasive capacity [Bindels et al., 2001; Kawanishi et al., 2008].

Cells are seeded on the Polyacrylamide gel (see below) and left overnight to spread. An image is acquired with a time interval of 60 sec for 2 hours.

Gel preparation

A protocol similar to the one reported in earlier works [Dembo and Wang, 1999; Pelham and Wang, 1999] has been used to produce 10 kPa PA gels. A square coverglass (22 mm × 22 mm) is treated with silane (Sigmacote SL-2) for 30 minutes. Round coverglasses (35 mm diameter) are washed with 0.1M NaOH, treated with APTMS for 10 minutes, washed with PBS twice and treated with 200 µl of 0.5% glutaraldehyde for 30 minutes. A 0.5 ml gel solution is prepared, containing 30% acrylamide (166 µl), 1% bis–acrylamide (14 µl) in distilled water (314 µl). Fluorescent beads (3 µl, Molecular Probes, 0.2 µm in diameter) are seeded into the solution before addition of the crosslinkers (2.5 µl of APS and 0.5 µl of TEMED). Overall, the gel contains 10% acrylamide and 0.03% bis–acrylamide. The adequate amount of solution (corresponding to a 70 µm gel thickness) is set onto the square coverglass. The circular coverglass is brought carefully from the top to capture the gel solution by capillarity, thus avoiding to flip the preparation. The gel is left to polymerize for nearly 90 minutes. After polymerization, the square coverglass is gently removed. In this protocol, Sulfo–Sanpah is used to covalently bind the protein (collagen) to the polyacrylamide surface. The gel is covered with 200 µl of a Sulfo–Sanpah solution (Sulfo–Sanpah 1mM, DMSO and HEPES at pH=8.5), then exposed to a UV lamp (2 × 15 Watts) for 2 mn: this enables to activate Sulfo–Sanpah molecules, so that they bind collagen. This process is repeated twice, then 200 µl of the collagen solution (100 µg/ml) are applied and let overnight to bind the activated Sulfo-Sanpah at 4 °C. To check the efficacy of the procedure, GFP–fibronectin was coated on the gels and it was shown that a uniform density was obtained (data not shown). Furthermore, T24 cell monolayers

were cultured on these gels and were shown to cover the whole surface.

The mechanical gel properties have been determined previously [Ambrosi et al., 2009] and the specific gel used throughout this study (10% acrylamide-0.03% bis–acrylamide) has an elastic Young modulus $E = 10\,\mathrm{kPa}$ as determined by rheometry, assuming that $\nu = 0.5$ (Poisson coefficient). This was also checked using AFM measurements [Peschetola, 2011]. The gel roughness was shown to be around 100 nm as shown using AFM contact mode. Note that the value of the gel rigidity (10 kPa) was selected as a compromise between stiffness of the physiological environment and the minimization of three–dimensional deformations that could occur for too soft gels. The value of 10 kPa appeared to meet these two conditions, and displacements were also easily detected (usually a few µm).

Traction forces

The mechanical characterization of the gel is approximated as isotropic and elastic and the displacements are observed to be small enough so that linear elasticity applies. The gel depth, usually 70 µm, is large enough (for the applied loads) so that it can be approximated by a half space. Since the response of the substrate is linear, the displacement $\mathbf{u}(\mathbf{r})$ at position $\mathbf{r}$ can be determined from the traction field $\mathbf{t}(\mathbf{r})$ at the boundary ($x_3 = 0$) of the 3D–gel via the integral:

$$\mathbf{u}(\mathbf{r}) = \int \mathbf{G}(\mathbf{r} - \mathbf{r}')\,\mathbf{t}(\mathbf{r}')\,\mathrm{d}s(\mathbf{r}') \tag{1}$$

where $\mathbf{G}$ is the Green's tensor for the Boussinesq–Cerruti problem [Landau and Lisfchitz, 1967], and the integral is operated on the surface between gel and cell. In the particular case where (1) is used for $\mathbf{r} = (x_1, x_2, 0)$ and pure shear $\mathbf{t} = (t_1, t_2, 0)$ applies, $\mathbf{G}(\mathbf{r})$ takes the form:

$$\mathbf{G}(\mathbf{r}) = \frac{1+\nu}{\pi E}\left((1-\nu)\,\frac{\mathbf{1}}{r} + \nu\,\frac{\mathbf{r}\otimes\mathbf{r}}{r^3}\right) \tag{2}$$

where r is the magnitude of $\mathbf{r}$, E is the elastic modulus, ν is the Poisson ratio, and $\mathbf{1}$ is the identity tensor.

In this work we use the adjoint method, whose details are given in previous works [Ambrosi, 2006; Ambrosi et al., 2009]. We recall that first, the problem is reduced to a 2D–one by averaging along an effective thickness h (in the x_3 direction). Secondly, the tractions are determined by a minimization technique, following Lions [Lions, 1968]. The solution method rewrites in solving the following partial differential equations and boundary conditions with unknowns $\mathbf{u}$ and the auxiliary unknown $\mathbf{p}$:

$$-\mu\Delta\mathbf{u} - (\mu+\lambda)\,\nabla(\nabla.\mathbf{u}) = -\frac{\chi_c}{\varepsilon}(\mathbf{p}-\bar{\mathbf{p}}) \quad \text{in} \quad \Omega_c, \qquad \mathbf{u}=\mathbf{0} \quad \text{on} \quad \partial\Omega_c \tag{3}$$

$$-\mu\Delta\mathbf{p} - (\mu+\lambda)\,\nabla(\nabla.\mathbf{p}) = \chi_0(\mathbf{u}-\mathbf{u_0}) \quad \text{in} \quad \Omega_c, \qquad \mathbf{p}=\mathbf{0} \quad \text{on} \quad \partial\Omega_c \tag{4}$$

In the above equations, $\bar{\mathbf{p}} = \frac{1}{|\Omega_c|}\int_{\Omega_c}\mathbf{p}\mathrm{d}s$, χ_c and χ_0 are characteristic functions associated to Ω_c (cell region) and Ω_0 (where beads displacements are known), $\mathbf{u_0}$ is the known displacement, $\mu = \frac{hE}{2(1+\nu)}$ and $\lambda = \frac{hE\nu}{1-\nu^2}$ are the reduced 2D–Lamé coefficients (plane stress model). h is chosen as the height within which beads significantly move (typically $h = 1.5\,\mu\mathrm{m}$). ε is the regularization parameter to be optimized using the L–curve technique [Ambrosi, 2006; Peschetola, 2011]. We used $\varepsilon = 6\times10^{-7}$ in our case.

Finally, the traction field $\mathbf{t}$ is given by $\mathbf{t} = -\frac{\chi_c}{\varepsilon}(\mathbf{p}-\bar{\mathbf{p}})$ [Peschetola, 2011], which ensures that the traction forces are null outside the cell, and that the resulting force on the cell is zero: $\int_{\Omega_c}\mathbf{t}\mathrm{d}s = \mathbf{0}$.

The observed displacement $\mathbf{u_0}$ is extracted from fluorescent images of the beads within the gel surface. The relaxed (i.e. Initial) beads positions are actually recovered at the end of the experiment by adding distilled water in the culture medium, which makes cells to detach and the gel eventually relaxes. Then the displacement $\mathbf{u_0}$ can be calculated, thanks to the trajectory reconstruction routine 'Particle–Tracker' available in the ImageJ package [Rasband, 1997].

The system of equations (3-4) is solved using a finite element method with elements nodes matching the beads positions. Then linear basis functions are used on an unstructured mesh. A biconjugate gradient method has been used to solve the resulting linear system numerically.

The trajectories are determined by following of the center of mass, while the resultant force is computed by integration of the stress times the surface element area (from the finite element mesh) to obtain the resultant force. Time–dependent results have been obtained by following cell trajectories, and traction stresses are presented using boxplots. Then outliers[1] representing the highest forces are extracted, and the mean value is taken from this data.

Cell migration on gels and Mean Squared Displacement (MSD)

Special Petri dishes with coverglass were used onto which PA gels (10 kPa) were prepared for the long–term migration experiments. Cells were seeded on the gels. Several cells were selected and followed in time for 2 hours with 5 mn time intervals. As previously, the center of mass was determined and recorded in time. Then the Mean Squared Displacement (MSD) was calculated according to the definition :

[1] values located outside the interval $[Q_1 - \alpha\,(Q_3-Q_1); Q_3 + \alpha\,(Q_3-Q_1)]$, where Q_1 is the lower quartile, Q_3 the higher quartile, and $\alpha = 1.5$

$$\mathrm{MSD}(t) = < |\mathbf{r}(t+\tau) - \mathbf{r}(\tau)|^2 >_\tau \quad (5)$$

In this formula, $\mathbf{r}(\tau)$ is an initial vector position chosen along the center of mass' path, and $\mathbf{r}(t+\tau)$ is another vector, from which the squared norm is calculated. Then the averaging brackets $<>_\tau$ are taken for all possible time lags τ ($0 \leq \tau \leq t$), i.e. the different positions of the cell center of mass (see supplemental material S7 for more precise information).

The behavior of this MSD in time was analyzed by comparing it to t^α, where α is the time–exponent or persistence parameter. It is known that values of $\alpha < 1$ correspond to sub–diffusive motions (anomalous motion), $\alpha = 1$ means diffusive motion (random walk), whereas $\alpha > 1$ is a super–diffusive motion (due to possible active cellular transport). The case $\alpha = 2$ is called the ballistic case (directional motion, cells encounter no obstacle and distance is proportional to time). Such exponents were measured during the migration assay and the final value of α was chosen as the time–average value.

The behavior of the MSD is an important feature of the cell migration process, as shown recently [Dieterich et al., 2008] because it can allow to determine the signature of a particular cell to migrate, change direction or polarize over long periods of time.

Immunofluorescence and confocal microscopy

Briefly, after being washed with PBS, cells were fixed using PFA (paraformaldehyde 3% in PBS) for 10 min, permeabilized with PBS containing 0.5% Triton X100 for 10 min, and then washed with PBS containing 0.2% saponin and 2% BSA. Fixed cells were then incubated with rabbit anti–myosin IIA (Biomedical Technologies Inc., USA) and mouse anti–human paxillin (clone 5H11, from Upstate Biotechnology, USA) for 30 min, and washed with PBS containing 0.2% saponin and 2% BSA. Cells were then stained with phalloidin Alexa Fluor-488 for actin, Hoechst 33342 for nuclei, Donkey anti-rabbit IgG (conjugated with Dylight 649, Jackson ImmunoResearch, USA), and Goat anti-Mouse IgG (labelled with Alexa Fluor–546, Molecular Probes, The Netherlands). The samples were imaged using a Zeiss LSM710 confocal microscope at the Institut Albert Bonniot. An X63 objective (oil, Plan-Apochromat DICIII, WD190m) was used for higher quality images. Images were 1024x1024, leading to a pixel resolution of 0.063 µm and subsequent area resolution 0.004 μm^2. This insures good accuracy for measurements of the focal areas.

Live cell imaging was carried out on a confocal microscope (Zeiss LSM), also at the Institut Albert Bonniot. T24 and RT112 cells were transfected for actin–GFP and time acquisitions were taken every two minutes, simultaneously with the fluorescent beads (red) acquisition, so that actin

localization and traction forces could be correlated. Co–localization analysis was produced using the ImageJ software [Rasband, 1997].

Results

Time dependence of traction forces

An image showing a T24 cell on a PA substrate is shown in Fig. 1. The cell develops a large lamellipodium and migrates from left to right (see also supplemental movie $S1$). A traction force map at this characteristic time ($t = 6$ mn) is also shown in Fig. 1. The force pattern (per unit surface) developed by this type of cancer cell reaches maximum values that are in the range of 150 Pa.

Cell migration is a time–dependent phenomenon [Ambrosi et al., 2009; Stricker et al., 2011], as cells pull on their focal adhesion points and then relax. This dynamics is shown in Fig. 2 where a time–dependent locomotion is depicted over 40 minutes. Values of stress magnitudes are reported in the form of a boxplot for each time (the same information is in the supplemental movie $S2$). As seen previously for this type of cell [Ambrosi et al., 2009], T24 cells usually exhibit a periodic motion, pulling strongly and then relaxing stresses, repeatedly. This type of motion is the so called five–step process (mesenchymal motion): development of protrusions, formation of adhesion and pulling, cell contraction, release of bonds at the rear and recycling [Sheetz et al., 1998]. Note that a large number of outliers are present, corresponding to the higher forces developed at focal sites. This will be studied below.

Analogous results are for less invasive RT112 cancer cells, shown in Fig. 3. The cell has a round shape, more likely resembling an ameboid type of motion (see also supplemental movie $S3$). Tractions are more homogeneous, and the values are larger than for T24 cells (Fig. 4). The outliers over 78 minutes do not change much (see also supplemental movie $S4$).

To compare the motion of the two types of cancer cells, only higher values (i.e. outliers probably corresponding to focal complexes [Balaban et al., 2001]) are retained in Fig. 5. RT112 cells developing higher average values of outliers (around 170 Pa) are compared to T24 cells (120 Pa). This analysis was carried out for $N = 9$ cells of each type and by averaging results for all times. This result is in agreement with previous works [Munevar et al., 2001; Indra et al., 2011] and could describe a possible way for invasive cells to move rapidly without exerting large forces.

Global force exerted on half–cell

The total force developed by cancer cells on the PA substrate in the direction of migration is

calculated integrating on half a cell only (indeed the resultant force over the cell domain is zero, i.e. $\int_{\Omega_c} \mathbf{t}\, \mathrm{d}s = \mathbf{0}$) and is shown in Fig. 6. One can estimate the difference between T24 and RT112 cells. Forces are concentrated at the leading edge or within the lamellipodium for T24 cancer cells, whereas centripetal stresses are located all around the edges in the case of RT112 cells, a migration behavior similar to some keratocytes [Burton et al., 1999].

Immunofluorescence: focal adhesions, actin and myosin

Immunofluorescence experiments are reported in figures 7–8. Several proteins involved during cell migration are selectively investigated: the actin structure (in green, using staining with Phalloidin Alexa 488), focal adhesion complexes (in red, using an anti–paxillin antibody) as well as myosin motors (in magenta, using an antibody for myosin IIA); finally the composite picture showing all sub–structures is presented, with the nuclei stained in blue (using Hoechst for DNA).

The two cell types exhibit different structural patterns. T24 cells show a thin cytoskeleton located close to the edges with interconnected stress fibers throughout the whole cell, whereas RT112 cells exhibit a wider actin network close to the edges. This phenomenon was also observed for other cells of the same lines (data not shown) with different shapes, and seems to be type–dependent rather than shape–dependent.

T24 cells show larger focal complexes, as evidenced by the paxillin staining, thus allowing for a more efficient motion. This is confirmed by precise quantitative determination of the total area of focal complexes, which was made relevant by normalizing according to cell area. The contours of focal areas were determined for several cells (N=9 for each cell line, approximately 60-70 areas per cell), and only large focal areas (>0.5 µm^2, 30-40 per cell) were kept. It was shown that T24 cells present significantly ($p<0.001$) larger focal areas (1.13 ± 0.05 µm^2) as compared to RT112 cells (0.86 ± 0.03 µm^2), see also Table 1. Good accuracy is obtained thanks to the high resolution of the pixel area size (0.004 µm^2, see 'Materials and Methods'). As T24 cells exhibit a larger spreading area (2200 µm^2, as compared to 1600 µm^2 for RT112 cells) on PA gels, it is therefore better to look at the average of the ratio $FAs/A(\%)$ (ratio of total focal areas FAs over cell area A) which was plotted as a bar–plot in Fig. 9, and this average is slightly higher for T24 cells. Apparently RT112 cells develop a smaller amount of focal complexes on soft gels, and therefore cannot move efficiently: they are more likely to move slowly than undergo rapid migration. Note that similar focal areas, showing periodic spatial fingers at the edges, have been previously observed when applying mechanical stresses [Paul et al., 2008] or under flow [Couzon et al., 2009].

Actin and myosin are co–localized at the periphery of both cell lines (see Fig. 7 and Fig. 8). Actin fibers organize in a cortical structure crossing the focal adhesions, and similarly for Myosin

IIA, especially for RT112 cells (Fig. 8). This seems to correlate with the development of large forces. In the case of T24 invasive cells, the organization of the actin cortex shows interconnections over the whole cell body, as for Myosin IIA. There are larger adhesion sites than with RT112 cells. Regarding colocalization of actin and myosin, it is clear from Figure 8 that a larger cortex of acto–myosin is shown in the case of RT112 cells (thickness around 5 µm), whereas T24 cells (Figure 7) only show thin acto–myosin structures (1–2 µm) at the cell rims. This is to be discussed in the next section.

Cell migration and MSD

The migration process of the two cell types (T24 and RT112) can be described in terms of the MSD function, as well as the velocity of migration. The MSD was determined as explained in section 2.4, while the velocity of migration was chosen as the length of the trajectory over time, in order to detect cells going back and forth over long times. A clear difference between the two cell types appears, in terms of kinematics, i.e. the persistence parameter α equals 1.57 for T24 cells, whereas it is only 1.21 for the less invasive RT112 cells (N=9). The velocity of migration follows the same trend and shows that invasive T24 cancer cells ($V = 0.38\,\mu$m/mn) are faster than the slow RT112 cells ($V = 0.17\,\mu$m/mn), as could be expected.

Discussion

The main results reported above are summarized in Table 1: values of the cell cytological grade, the average magnitude of traction stresses outliers σ (in Pa), the average magnitude of the resultant force F (nN) developed on a half–cell, the ratio of focal adhesions to cell area $FAs/A(\%)$, the focal adhesions average area FAs (μm^2), the migration velocity $V(\mu$m/mn), and finally α, the exponent from the MSD relationship in Eq. (5). The value of the significance parameter p is also indicated.

Few studies have focused on the comparison between different cell lines behaviors on soft gels. Previous authors [Munevar et al., 2001] considered normal and H–ras transformed 3T3 fibroblasts. H–ras transformed cells were used previously [Bondy et al., 1985]. The H-ras gene was shown to alter the cells by developping metastatic ability. Indeed, cells (NIH3T3) transfected with the T24 human H-ras oncogene (pT24-C3) were able to grow *in vivo*, within an immunodeficient embryonic chick tissue, whereas other control NIH3T3 cells did not proliferate. Munevar *et al.* showed an unexpected behavior of H–ras fibroblasts which did not develop stable forces but rather disorganized values around the cell edges during motion. The same behavior is observed in this work with an increase of traction stresses with the less invasive cells (Fig. 5–6).

Another important aspect investigated here is the time–dependence of the traction forces for

the two cell types observed in Fig. 2 and Fig. 4. Outliers represented in these figures contain the information on the large forces developed at focal sites. The dynamics of outlier forces correspond to a classical five–step process [Sheetz et al., 1998] in the case of T24 cancer cells, as already noticed [Ambrosi et al., 2009]: forces peaks (as observed in Fig. 2) range from 80 Pa to 150 Pa roughly, with an average value around 120 Pa (Table 1). On the other hand, RT112 cells present outliers (in the time range considered) which remain rather constant (Fig. 4), equal to 171 Pa (Table 1), with very small fluctuations. This suggests that the motion described is continuous, where adhesions are rapidly formed and broken. This is also confirmed by inspection of Fig. 6, where local stresses on both sides of RT112 cells cancel out to give a resultant force in the direction of migration, as observed previously for keratocytes [Burton et al., 1999]. Therefore, a distinct mechanism of migration was observed for these two cell types and quantified. To investigate this characterization further, we analyze the location, number and size of focal adhesion areas (Fig. 9); they are known to be linked to the cytoskeleton, in particular the actin filaments. We measure the total area of paxillin–rich domains, in particular those with size larger than 0.5 μm^2 (mature adhesion sites). The percentage of focal areas with respect to cell size is shown and, interestingly, this fraction (around 1% for T24 cells, and 0.9% for RT112 cells, see Fig. 9) increases with cell invasivity. Moreover, significantly larger adhesion sites (1.13 μm^2) are found for T24 cells as compared to RT112 cells (0.86 μm^2, $p<0.001$, see Table 1). In another work [Indra et al., 2011], adhesion centrifugation assays conducted on harder PA gels showed a smaller number of adhering cells when metastatic capacity increased, but focal adhesions were only shown on glass substrates, so results are therefore difficult to compare in size and number of focal adhesion sites. Nevertheless, our data confirm that traction forces are not proportional to focal adhesion areas, a framework previously described earlier [Stricker et al., 2011] in the early stages of myosin–mediated maturation of adhesions. This means that these data concern probably cells showing focal adhesions at a different level of maturation, probably more mature ones.

The role of the cytoskeleton is clarified by studying fluorescent actin–images, and their correlation with the myosin and paxillin sub–structures in Figs 7–8. The interplay between actin and myosin enables cell contraction and allows motility (see for example [Aratyn-Schaus and Gardel, 2010]). Another correlation is between traction forces and the actin flow [Gardel et al., 2008] in regions where large focal areas exist and where the actin flow is small (and conversely). The myosin activity is usually linked to focal adhesions formation in the actin–rich lamellipodium [Giannone et al., 2007]. In the images showing myosin IIA and the actin network (Figs 7–8), it can be seen that the myosin IIA density is particularly enhanced at the leading edge of the cancer cells, and that it corresponds to the rich actin domains. On the other hand, the actin and myosin regions are

thin in the case of T24 cells (usually 1–2 μm wide), whereas they are large for RT112 cells (around 5 μm) thus allowing stronger acto–myosin contractions. This feature was also observed in other cases (figures not shown) and is in agreement with the actin–localization in Figures 10-11.

Focal areas located at the leading edge of T24 or RT112 cells differ: they are well connected to the actin and myosin networks for T24 cells, whereas they do not appear to be so well colocalized for RT112 cells. This difference could be explained as follows: focal complexes are not so important for less invasive RT112 cells, which mostly spread rather than migrate. On the contrary, T24 cells need to develop their mature adhesions rapidly and renew them faster, which makes them migrate more rapidly. This has been taken care of by using a precise criterion (focal area $> 0.5\,\mu\text{m}^2$) which insures quantification of mature focal adhesions, as opposed to unmature ones.

In terms of cell migration, the MSD analysis confirmed that T24 cells move more rapidly than less invasive RT112 cells and that their persistence exponent α is larger (1.57 for T24 cells *vs*. 1.21 for RT112 cells). The exponent of T24 cell is comparable to previous ones [Dieterich et al., 2008] who measured super–diffusive behaviors as well ($\alpha \sim 1.5$). Therefore this gel stiffness is a good candidate to differentiate these cells.

Finally, traction force microscopy in time is compared with the evolution of the actin cytoskeleton [Versaevel et al., 2012]. This was achieved thanks to actin–GFP transfected T24 and RT112 cells, and observations of the migration behavior was followed in time as before. Figures 10-11 show images of both the actin filaments and the magnitude of the forces developed by the two cancer cells (see also supplemental movies $S5$ and $S6$ for a more detailed time–dependent process). A good correlation appears between the actin density and the high levels of forces. In particular, Figure 11 shows a particularly large actin cortex developed by RT112 cells at the front, as seen before (Fig. 8): the larger forces are also located in that area. On the contrary, T24 cells as in Fig. 10 show a thinner cortex (same as previously, Fig. 7) with orientation following cell edges. This can be shown in the comparison of the intensity levels shown along the two lines in Figures 10-11 where a more defined actin intensity is seen at the cell edges for the T24 cell, whereas the actin cortex is wider for the RT112 cell. This result supports the idea that the two types of motion correspond to a clear different contractility: pulling at the front on adhesion sites for T24 cells, whereas RT112 cells pull on the sides thanks to larger acto–myosin complexes and use less adhesion.

This effect is detailed in Figure 12 where colocalization of the actin density is compared with the magnitude of traction stresses. As can be shown in these two figures, colocalization of actin (in green) and force (in red) is strong at the leading edge of T24 cell, whereas it is located in wider areas in the case of the RT112 cell. As suggested before, this feature seems to indicate that RT112 cells move by using large lateral contractions due to the presence of a wide acto–myosin cortex,

whereas T24 cells only use protrusions at the leading edge where the acto–myosin cortex is more efficient. This is a possible way to explain, at such cell levels, differences in the invasiveness of these two cell lines. Finally the ability to move faster might be controlled by the type of adhesive molecules involved, and their affinity to the extra–cellular–matrix; this work is presently under way.

Finally, despite the fact that the results obtained in this work can help to discrimate between more or less invasive cancer cells, the 3D aspects have been ignored here. Therefore one needs to be careful about generalizing these results in three dimensions. Indeed, some differences may appear. One should consider cells on 2D–substrates as well as cells embedded in a 3D environment, as previously described [Kraning-Rush et al., 2012; Koch et al., 2012]. Strictly speaking, all the latter methods are capable of giving information about cellular tractions but only qualitatively, except another recent work [Legant et al., 2010], where a single case of cell migration is computed. Some interesting tendencies have also been observed by studying the velocity of migration of cells embedded in matrigels [Zaman et al., 2006] to show the effects of ECM density, adhesions and matrix rigidity. It was shown that the pore size of the matrigel plays a key role in cell migration and leads to an important proteolytic activity. Definitely, there remains a big challenge in transfering this work into the third dimension and compare the 3D–invasiveness or metastatic ability of such cells to invade another medium, while computing associated forces.

Conclusions

The motility of two types of epithelial bladder cancer cells has been investigated from a biophysical point of view. These cells present different invasive behavior, in particular T24 cells are more invasive than RT112 cells. Substrates of PolyAcrylamide (stiffness $\sim 10\,\mathrm{kPa}$) have been chosen to perform all studies. The results concern the relationship between focal areas, cytoskeleton structure, migration velocities and forces exerted by cells thanks to Traction Force Microscopy (TFM). The main conclusions are that invasive cells (T24) need less traction forces to migrate, and exhibit an organized cytoskeleton (actin and myosin structures) with large dynamic adhesion sites, resulting in larger migration velocities on this particular substrate. On the other hand, less invasive RT112 cells exert larger forces thanks to a wide acto–myosin cortex, with smaller focal adhesions. The applications of this method could be an interesting *in vitro* tool to test the invasivity of different cancer cells; in particular, the role of traction stress may provide a possible classification criterion.

Future studies could focus on the optimization of protocols (choice of substrate, functionnal-

ization, topography) with high numbers of cells. Finally, promising current work is ongoing to relate the possible proteins involved in cancer migration of such cells [Chotard-Ghodsnia et al., 2007; Haddad et al., 2010], like $\beta 1$ integrins [Indra et al., 2011] or $\alpha 5 - \beta 1$ [Mierke et al., 2011] and more precisely chemokine CXCL1 in the case of the two lines studied here [Kawanishi et al., 2008]. This would enhance the current results on the traction forces measured here by TFM. Possibly this could also enable models [Mogilner and Keren, 2009; Verdier et al., 2009; Herant and Dembo, 2010; Shao et al., 2010; Etienne and Duperray, 2011] to predict cancer cell shapes during migration.

And last, but not the least, it is now necessary to compute traction forces in three dimensions [Legant et al., 2010], in order to focus on the mechanisms and forces developped by cancer cells to migrate into tissues.

Acknowledgments

We are thankful to the Université Franco–Italienne and to the European Commission (Marie Curie Research Training Network, MRTN–CT–2004–503661). Confocal microscopy was performed at the microscopy facility of the Institut Albert Bonniot, thanks to grants "Association pour la Recherche sur le Cancer" (ARC, Villejuif, France) and the Nanobio program (Nanosciences Foundation, Grenoble). We thank Olivier Destaing for help with the transfection of actin–GFP.

References

Ambrosi D. 2006. Cellular traction as an inverse problem. SIAM J Appl Math 66:2049–2060.

Ambrosi D, Duperray A, Peschetola V, Verdier C. 2009. Traction patterns of tumor cells. J Math Biol 58:163–181.

Aratyn-Schaus Y and Gardel ML. 2010. Transient frictional slip between integrin and the ECM in focal adhesions under myosin II tension. Current Biology 20(13):1145–1153.

Balaban NQ, Schwarz US, Riveline D, Goichberg P, Tzur G, Sabanay I, Mahalu D, Safran S, Bershadsky A, Addadi L, Geiger B. 2001. Force and focal adhesion assembly: a close relationship studied using elastic micropatterned substrates. Nat Cell Biol 3(5):466–472.

Bindels EM, Vermey M, De Both NJ, van der Kwast TH. 2001. Influence of the microenvironment on invasiveness of human bladder carcinoma cell lines. Virchows Arch 439(4):552–559.

Bondy GP, Wilson S, Chambers AF. 1985. Experimental metastatic ability of H–ras–transformed NHI3T3 cells. Cancer Research 45(4):6005–6009.

Burton K and Taylor DL. 1997. Traction forces of cytokinesis measured with optically modified elastic substrata. Nature 385(6615):450–454.

Burton K, Park JH, Taylor DL. 1999. Keratocytes generate traction forces in two phases. Mol Biol Cell 10(11):3745–3769.

Butler JP, Tolic-Norrelykke IM, Fabry B, Fredberg JJ. 2002. Traction fields, moments, strain energy that cells exert on their surroundings. Am J Physiol Cell Physiol 282(3):C595–C605.

Choquet D, Felsenfeld DP, Sheetz MP. 1997. Extracellular matrix rigidity causes strengthening of integrin-cytoskeleton linkages. Cell 88(1):39–48.

Chotard-Ghodsnia R, Haddad O, Leyrat A, Drochon A, Verdier C, Duperray A. 2007. Morphological analysis of tumor cell/endothelial cell interactions under shear flow. J Biomech 40(2): 335–344.

Couzon C, Duperray A, Verdier C. 2009. A critical stress to detach cancer cells in microchannels. Eur Biophys J 38:1035–1047.

Delanoë-Ayari H, Rieu J.-P, Sano M. 2010. 4D traction force microscopy reveals asymmetric cortical forces in migrating dictyostelium cells. Phys Rev Lett 105:248103.

Dembo M and Wang YL. 1999. Stresses at the cell-to-substrate interface during locomotion of fibroblasts. Biophys J 76(4):2307–2316.

Dieterich P, Klages R, Preuss R, Schwab A. 2008. Anomalous dynamics of cell migration. Proc Natl Acad Sci USA 105(2):459–463.

Discher DE, Janmey P, Wang YL. 2005. Tissue cells feel and respond to the stiffness of their substrate. Science 310(5751):1139–1143.

Etienne J and Duperray A. 2011. Initial dynamics of cell spreading are governed by dissipation in the actin cortex. Biophys J 101(3):611–621.

Fournier MF, Sauser R, Ambrosi D, Meister JJ, Verkhovsky AB. 2010. Force transmission in migrating cells. J Cell Biol 188(2):287–297.

Friedl P, Borgmann S, Bröcker EB. 2001. Amoeboid leukocyte crawling through extracellular matrix: lessons from the dictyostelium paradigm of cell movement. J Leukoc Biol 70(4):491–509.

Galbraith CG, Yamada KM, Sheetz MP. 2002. The relationship between force and focal complex development. J Cell Biol 159(4):695–705.

Gardel ML, Sabass B, Ji L, Danuser G, Schwarz US, Waterman CM. 2008. Traction stress in focal adhesions correlates biphasically with actin retrograde flow speed. J Cell Biol 183(6): 999–1005.

Ghibaudo M, Saez A, Trichet L, Xayaphoummine A, Browaeys J, Silberzan P, Buguin A, Ladoux B. 2008. Traction forces and rigidity sensing regulate cell functions. Soft Matter 4: 1836–1843.

Ghibaudo M, Trichet L, Digabel JL, Richert A, Hersen P, Ladoux B. 2009. Substrate topography induces a crossover from 2D to 3D behavior in fibroblast migration. Biophys J 97(1):357–368.

Giannone G, Dubin-Thaler BJ, Rossier O, Cai Y, Chaga O, Jiang G, Beaver W, Döbereiner HG, Freund Y, Borisy G, Sheetz MP. 2007. Lamellipodial actin mechanically links myosin activity with adhesion-site formation. Cell 128(3):561–575.

Gupton SL and Waterman-Storer CM. 2006. Spatiotemporal feedback between actomyosin and focal–adhesion systems optimizes rapid cell migration. Cell 125(7):1361–1374.

Haddad O, Chotard-Ghodsnia R, Verdier C, Duperray A. 2010. Tumor cell/endothelial cell tight contact upregulates endothelial adhesion molecule expression mediated by NF–κB: differential role of the shear stress. Exp Cell Research 316:615–626.

Harris AK, Wild P, Stopak D. 1980. Silicone rubber substrata: a new wrinkle in the study of cell locomotion. Science 208:177–179.

Herant M and Dembo M. 2010. Form and function in cell motility: from fibroblasts to keratocytes. Biophys J 98(8):1408–1417.

Indra I, Undyala V, Kandow C, Thirumurthi U, Dembo M, Beningo KA. 2011. An in vitro correlation of mechanical forces and metastatic capacity. Phys Biol 8(1):015015.

Iordan A, Duperray A, Gérard A, Grichine A, Verdier C. 2010. Breakdown of cell-collagen networks through collagen remodeling. Biorheology 47:277–295.

Kawanishi H, Matsui Y, Ito M, Watanabe J, Takahashi T, Nishizawa K, Nishiyama H, Kamoto T, Mikami Y, Tanaka Y, et al. 2008. Secreted CXCL1 is a potential mediator and marker of the tumor invasion of bladder cancer. Clin Cancer Res 14(9):2579–2587.

Keren K, Pincus Z, Allen GM, Barnhart EL, Marriott G, Mogilner A, Theriot JA. 2008. Mechanism of shape determination in motile cells. Nature 453(7194):475–480.

Koch TM, Mnster S, Bonadkar N, Butler JP, Fabry B. 2012. 3D Traction forces in cancer cell invasion. PLoS One 7(3):e33476.

Kraning-Rush CM, Califano JP, Reinhart-King CA. 2012. Cellular traction stresses increase with increasing metastatic potential. Plos One 7(2):e32572.

Landau L and Lisfchitz E. 1967. Théorie de l'élasticité. Editions Mir, Moscow.

Legant WR, Miller JS, Blakely BL, Cohen DM, Genin GM, Chen CS. 2010. Measurement of mechanical tractions exerted by cells in three-dimensional matrices. Nat Methods 7(12):969–971.

Lions JL. 1968. Contrôle optimal de systèmes gouvernés par des équations aux dérivées partielles. Dunod, Paris.

Lo CM, Wang HB, Dembo M, Wang YL. 2000. Cell movement is guided by the rigidity of the substrate. Biophys J 79(1):144–152.

Maskarinec SA, Franck C, Tirrell DA, Ravichandran G. 2009. Quantifying cellular traction forces in three dimensions. Proc Natl Acad Sci USA 106(52):22108–22113.

Michel R, Peschetola V, Bedessem B, Etienne J, Ambrosi D, Duperray A, Verdier C. 2012. Inverse problems for the determination of traction forces by cells on a substrate: a comparison of two methods. Comput Methods Biomech Biomed Eng 15:(S1):27–29.

Mierke CT, Rösel D, Fabry B, Brábek J. 2008. Contractile forces in tumor cell migration. Eur J Cell Biol 87:669–676.

Mierke CT, Frey B, Fellner M, Herrmann M, Fabry B. 2011. Integrin alpha5–beta1 facilitates cancer cell invasion through enhanced contractile forces. J Cell Sci 124(3):369–383.

Mogilner A and Keren K. 2009. The shape of motile cells. Current Biology 19:R762–R771.

Munevar S, Wang Y, Dembo M. 2001. Traction force microscopy of migrating normal and h-ras transformed 3T3 fibroblasts. Biophys J 80(4):1744–1757.

Palecek SP, Loftus JC, Ginsberg MH, Lauffenburger DA, Horwitz AF. 1997. Integrin-ligand binding properties govern cell migration speed through cell-substratum adhesiveness. Nature 385(6616):537–540.

Paul R, Heil P, Spatz JP, Schwarz US. 2008. Propagation of mechanical stress through the actin cytoskeleton toward focal adhesions: model and experiment. Biophys J 94(4):1470–1482.

Pelham RJ and Wang Y. 1999. High resolution detection of mechanical forces exerted by locomoting fibroblasts on the substrate. Mol Biol Cell 10(4):935–945.

Peschetola V. 2011. Traction forces exerted by cancer cells migrating on gels. PhD thesis, Université de Grenoble.

Pollard TD and Borisy GG. 2003. Cellular motility driven by assembly and disassembly of actin filaments. Cell 112(4):453–465.

Rasband WS. 1997. ImageJ. U.S. National Institutes of Health, Bethesda, Maryland, USA.

Sabass B, Gardel ML, Waterman CM, Schwarz US. 2008. High resolution traction force microscopy based on experimental and computational advances. Biophys J 94(1):207–220.

Saez A, Ghibaudo M, Buguin A, Silberzan P, Ladoux B. 2007. Rigidity-driven growth and migration of epithelial cells on microstructured anisotropic substrates. Proc Natl Acad Sci USA 104(20):8281–8286.

Schwarz US, Balaban NQ, Riveline D, Bershadsky A, Geiger B, Safran SA. 2002. Calculation of forces at focal adhesions from elastic substrate data: the effect of localized force and the need for regularization. Biophys J 83(3):1380–1394.

Shao D, Rappel WJ, Levine H. 2010. Computational model for cell morphodynamics. Phys Rev Lett 105:108104.

Sheetz MP, Felsenfeld DP, Galbraith CG. 1998. Cell migration: regulation of force on extracellular-matrix-integrin complexes. Trends Cell Biol 8(2):51–54.

Stricker J, Sabass B, Schwarz US, Gardel ML. 2010. Optimization of traction force microscopy for micron-sized focal adhesions. J Phys Condens Matter 22(19):194104.

Stricker J, Aratyn-Schaus Y, Oakes PW, Gardel ML. Spatiotemporal constraints on the force-dependent growth of focal adhesions. Biophys J 100(12):2883–2893, 2011.

Tan JL, Tien J, Pirone DM, Gray DS, Bhadriraju K, Chen CS. 2003. Cells lying on a bed of microneedles: an approach to isolate mechanical force. Proc Natl Acad Sci USA 100(4): 1484–1489.

Verdier C, Etienne J, Duperray A, Preziosi L. 2009. Review: Rheological properties of biological materials. C R Acad Sci Phys 10:790–811.

Versaevel M, Grevesse T, Gabriele S. 2012. Spatial coordination between cell and nuclear shape within micropatterned endothelial cells. Nat Commun 3(671):1–12.

Zaman MH, Trapani LM, Siemeski AL, Mackellar D, Gong H, Kamm RD, Wells A, Lauffenberger DA, Matsudaira P. 2006. Migration of tumor cells in 3D matrices is governed by matrix stiffness along with cell-matrix adhesion and proteolysis. Proc Natl Acad Sci USA 103(29): 10889–10894.

Table captions

Table 1. Summary of dynamic and kinematic quantities obtained for T24 and RT112 cells. Values of the cell cytological grade, the average magnitude of traction stresses outliers σ (in Pa), the average magnitude of the resultant force F (nN) developed on a half–cell, the ratio of focal adhesions to cell area $FAs/A(\%)$, the focal adhesions average area FAs (μm^2), the migration velocity $V(\mu m/mn)$, and finally α, the exponent from the MSD relationship in Eq. (5). The value of the significance parameter p is also indicated. (*) $p< 0.05$, (**) $p< 0.01$ and (***) for $p< 0.001$.

Figure captions

Figure 1. Phase–contrast image of a T24 cancer cell and corresponding traction field. Time $t = 6$ min from Fig. 2. The traction field is represented as a color map. The color scale for stresses reads in Pascal (Pa).

Figure 2. Time variation of the magnitude of traction stresses exerted by a T24 migrating cancer cell. The representation is made as a Boxplot. The lines in the Boxplot correspond to 25%, 50%, 75%, and the whiskers extend to the 1.5 interquartile range. Outliers are above. The mean value for each time step is indicated by the red dots.

Figure 3. Phase–contrast image of a RT112 cancer cell and corresponding traction field. Time $t = 18$ min from Fig. 4. The traction field is represented as a color map. The color scale for stresses reads in Pascal (Pa).

Figure 4. Time variation of the magnitude of traction stresses exerted by a RT112 migrating cancer cell. The representation is made as a Boxplot. The lines in the Boxplot correspond to 25%, 50%, 75%, and the whiskers extend to the 1.5 interquartile range. Outliers are above. The mean value for each time step is indicated by the red dots.

Figure 5. Mean value of the outliers of traction stresses for T24 and RT112 cell lines. The data is shown as the mean + standard error about the mean (SEM). The difference among the mean value is significant according to the GEE test ($p = 0.0069$).

Figure 6. Stresses in a half–cell and resultant. T24 cell (above), RT112 cell (middle) and bar–plot (below) showing time-average force in the direction of migration ($p = 0.14$). The arrow shows the resultant (direction and magnitude).

Figure 7. Fluorescent images of T24 cancer cells adhering on PA gel. Gel stiffness is 10kPa. From left to right and top to bottom: cells are stained for actin with Phalloidin Alexa 488 (green), anti–paxillin for focal adhesion sites (red), anti–myosin antibody for myosin IIA (magenta) and Hoechst for nuclei (blue).

Figure 8. Fluorescent images of RT112 cancer cells adhering on PA gel. Gel stiffness is 10kPa). From left to right and top to bottom: cells are stained for actin with Phalloidin Alexa 488 (green), anti–paxillin for focal adhesion sites (red), anti–myosin antibody for myosin IIA (magenta) and Hoechst for nuclei (blue).

Figure 9. Focal adhesions. A: Microscopy image of focal adhesions. **B:** Details of segmentation procedure for focal adhesions calculation. Bar–plot representing total area of focal complexes (>0.5 µm^2) divided by cell area ($p = 0.25$). See also Table 1 for details.

Figure 10. Image of T24 cancer cell transfected for actin. PA gel substrate of stiffness 10kPa. Fluorescent image with insert indicating the level of actin expression for the line drawn. Corresponding traction force map (in Pa).

Figure 11. Image of RT112 cancer cell transfected for actin. PA gel substrate of stiffness 10kPa. Fluorescent image with insert indicating the level of actin expression for the line drawn. Corresponding traction force map (in Pa).

Figure 12. Colocalization of the actin and force levels. T24 cell (top) and RT112 cell (below). Larger actin areas are found with the RT112 cell.

Supplemental materials

Supplemental movie S1. Phase–contrast movie of a migrating T24 cancer cell. Time lapse is one image every 2 minutes.

Supplemental movie S2. Corresponding traction field of the migrating T24 cell. Representation as a color map. The color scale for stresses reads in Pascal (time lapse is one image every 2 minutes).

Supplemental movie S3. Phase–contrast movie of a migrating RT112 cancer cell. Time lapse is one image every 4 minutes.

Supplemental movie S4. Corresponding traction field of the migrating RT112 cell represented as a color map. The color scale for stresses reads in Pascal (one image every 4 minutes).

Supplemental movie S5. Colocalization map of actin fibers and stress magnitude for migrating T24 cell. Time lapse is one image per 2 minutes.

Supplemental movie S6. Colocalization map of actin fibers and stress magnitude for migrating RT112 cell. Time lapse is one image per 2 minutes.

Supplement S7. Information for the Mean Square Displacement (MSD).

Table

Cell type	Cyt. grade	σ (Pa)	F(nN)	FAs/A(%)	FAs(µm^2)	V(µm/mn)	α
T24	G3	120	17.4	0.98	1.13	0.38	1.57
RT112	G2	171	22.8	0.89	0.86	0.17	1.21
p	-	(**)	0.14	0.4	(***)	(***)	(***)

Table 1: **Summary of dynamic and kinematic quantities obtained for T24 and RT112 cells**. Values of the cell cytological grade, the average magnitude of traction stresses outliers σ (in Pa), the average magnitude of the resultant force F (nN) developed on a half–cell, the ratio of focal adhesions to cell area FAs/A(%), the focal adhesions average area FAs (µm^2), the migration velocity V(µm/mn), and finally α, the exponent from the MSD relationship in Eq. (5). The value of the significance parameter p is also indicated. (*) p$<$ 0.05, (**) p$<$ 0.01 and (***) for p$<$ 0.001.

Figures

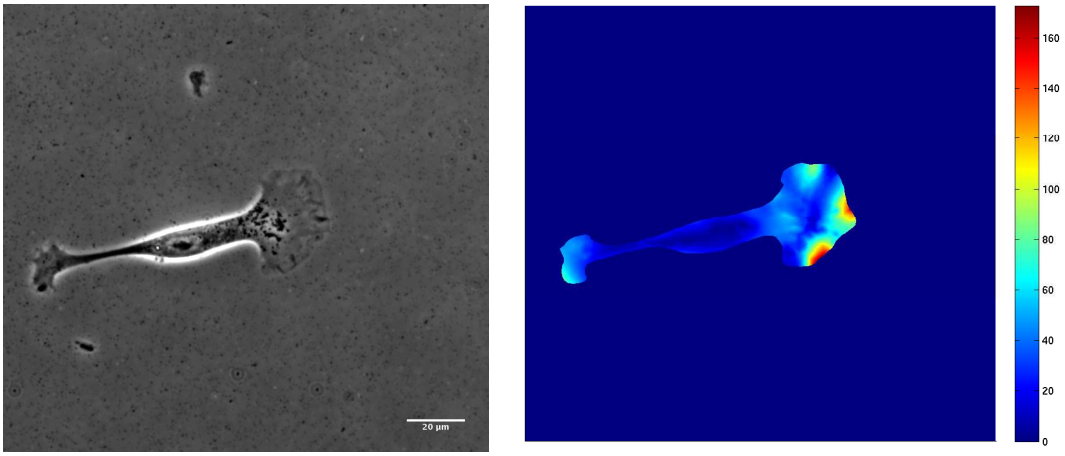

Figure 1: **Phase–contrast image of a T24 cancer cell and corresponding traction field.** Time $t = 6$ min from Fig. 2. The traction field is represented as a color map. The color scale for stresses reads in Pascal (Pa).

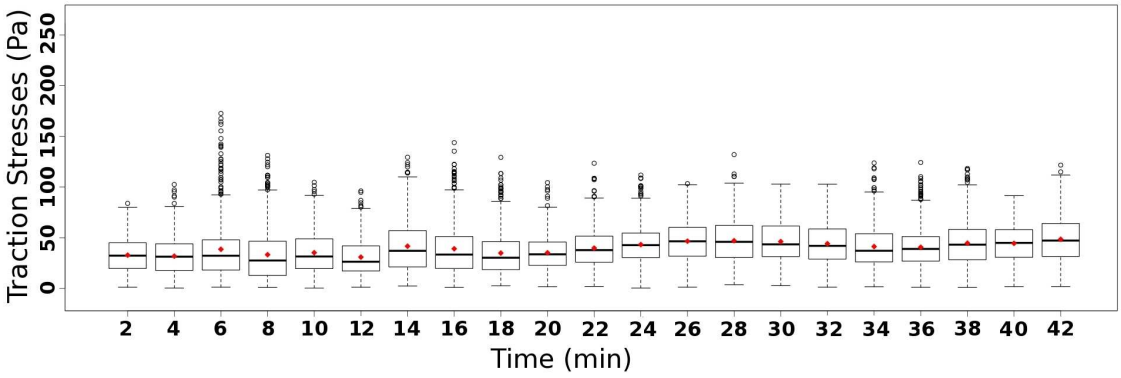

Figure 2: **Time variation of the magnitude of traction stresses exerted by a T24 migrating cancer cell.** The representation is made as a Boxplot. The lines in the Boxplot correspond to 25%, 50%, 75%, and the whiskers extend to the 1.5 interquartile range. Outliers are above. The mean value for each time step is indicated by the red dots.

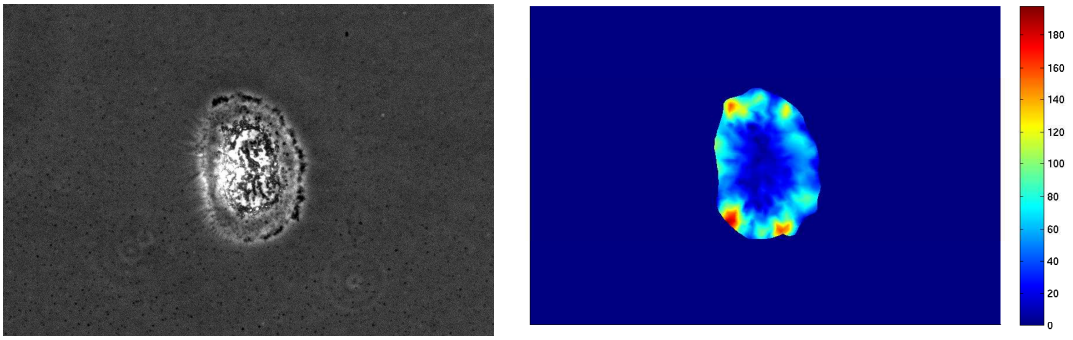

Figure 3: **Phase–contrast image of a RT112 cancer cell and corresponding traction field.** Time $t = 18$ min from Fig. 4. The traction field is represented as a color map. The color scale for stresses reads in Pascal (Pa).

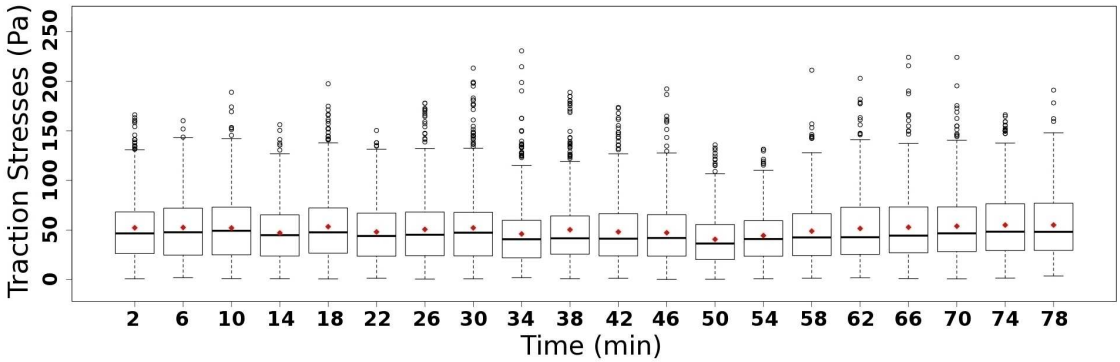

Figure 4: **Time variation of the magnitude of traction stresses exerted by a RT112 migrating cancer cell.** The representation is made as a Boxplot. The lines in the Boxplot correspond to 25%, 50%, 75%, and the whiskers extend to the 1.5 interquartile range. Outliers are above. The mean value for each time step is indicated by the red dots.

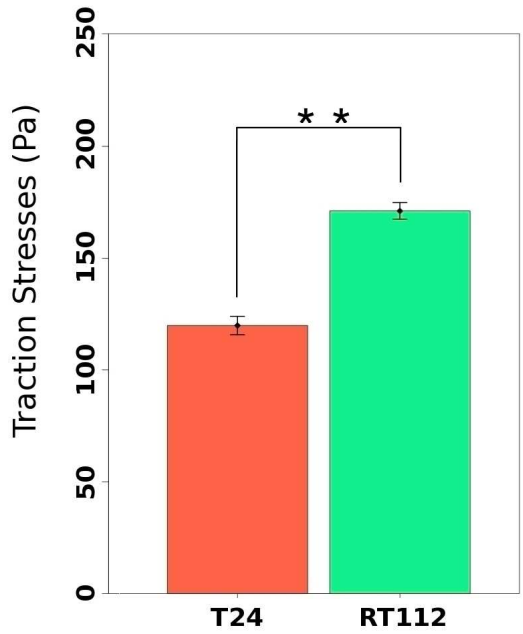

Figure 5: **Mean value of the outliers of traction stresses for T24 and RT112 cell lines.** The data is shown as the mean + standard error about the mean (SEM). The difference among the mean value is significant according to the GEE test ($p = 0.0069$).

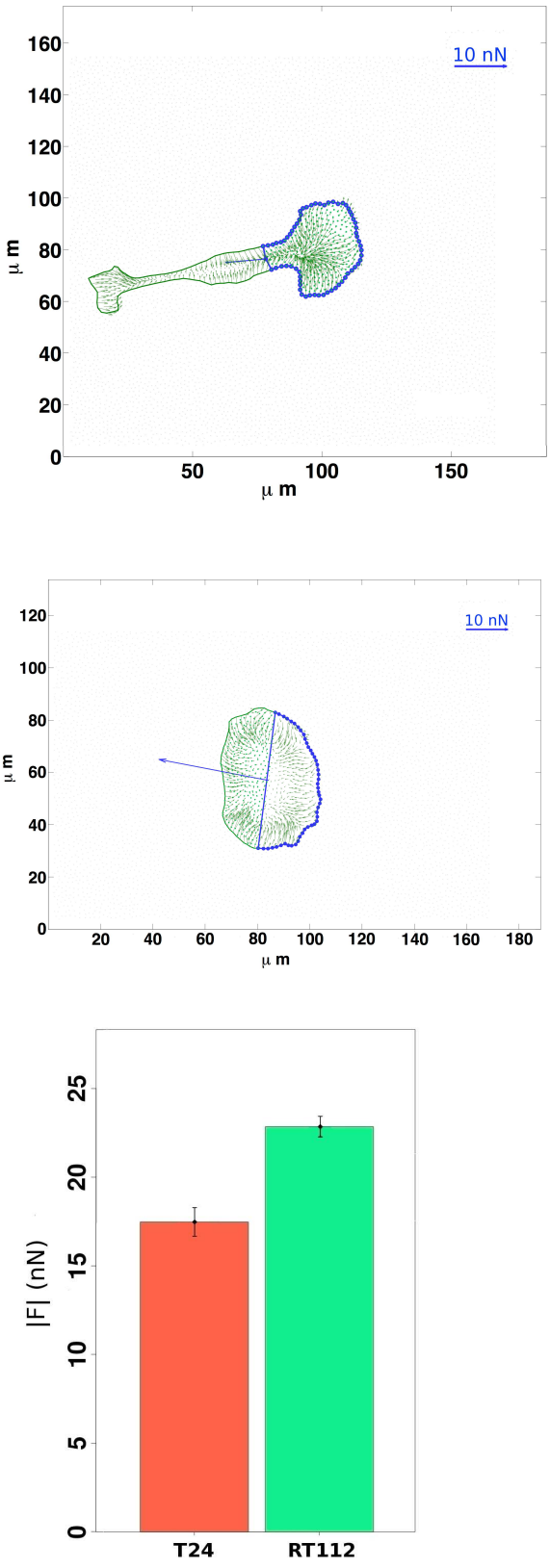

Figure 6: **Stresses in a half–cell and resultant.** T24 cell (above), RT112 cell (middle) and bar–plot (below) showing time-average force in the direction of migration ($p = 0.14$). The arrow shows the resultant (direction and magnitude).

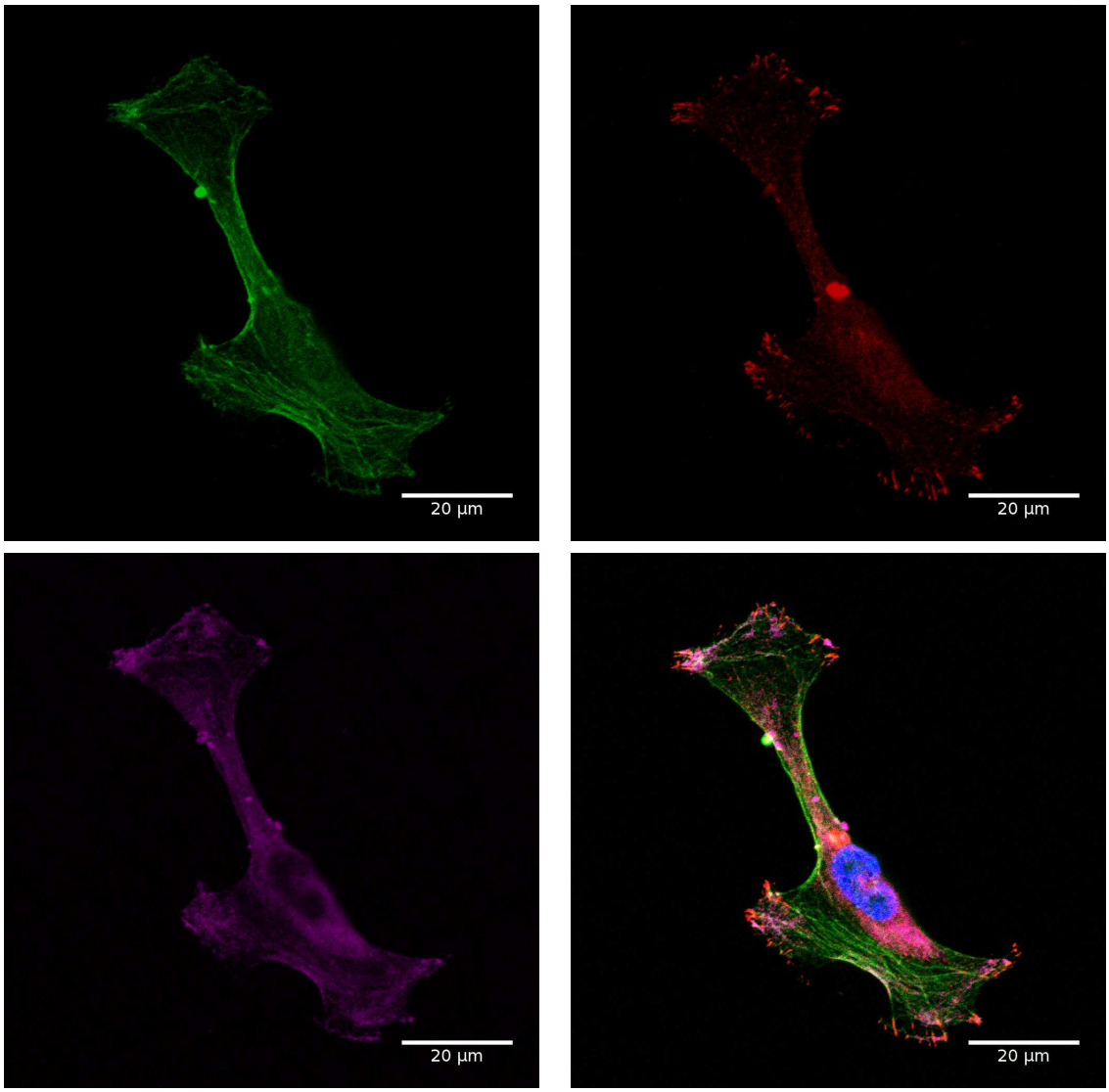

Figure 7: **Fluorescent images of T24 cancer cells adhering on PA gel.** Gel stiffness is 10kPa. From left to right and top to bottom: cells are stained for actin with Phalloidin Alexa 488 (green), anti–paxillin for focal adhesion sites (red), anti–myosin antibody for myosin IIA (magenta) and Hoechst for nuclei (blue).

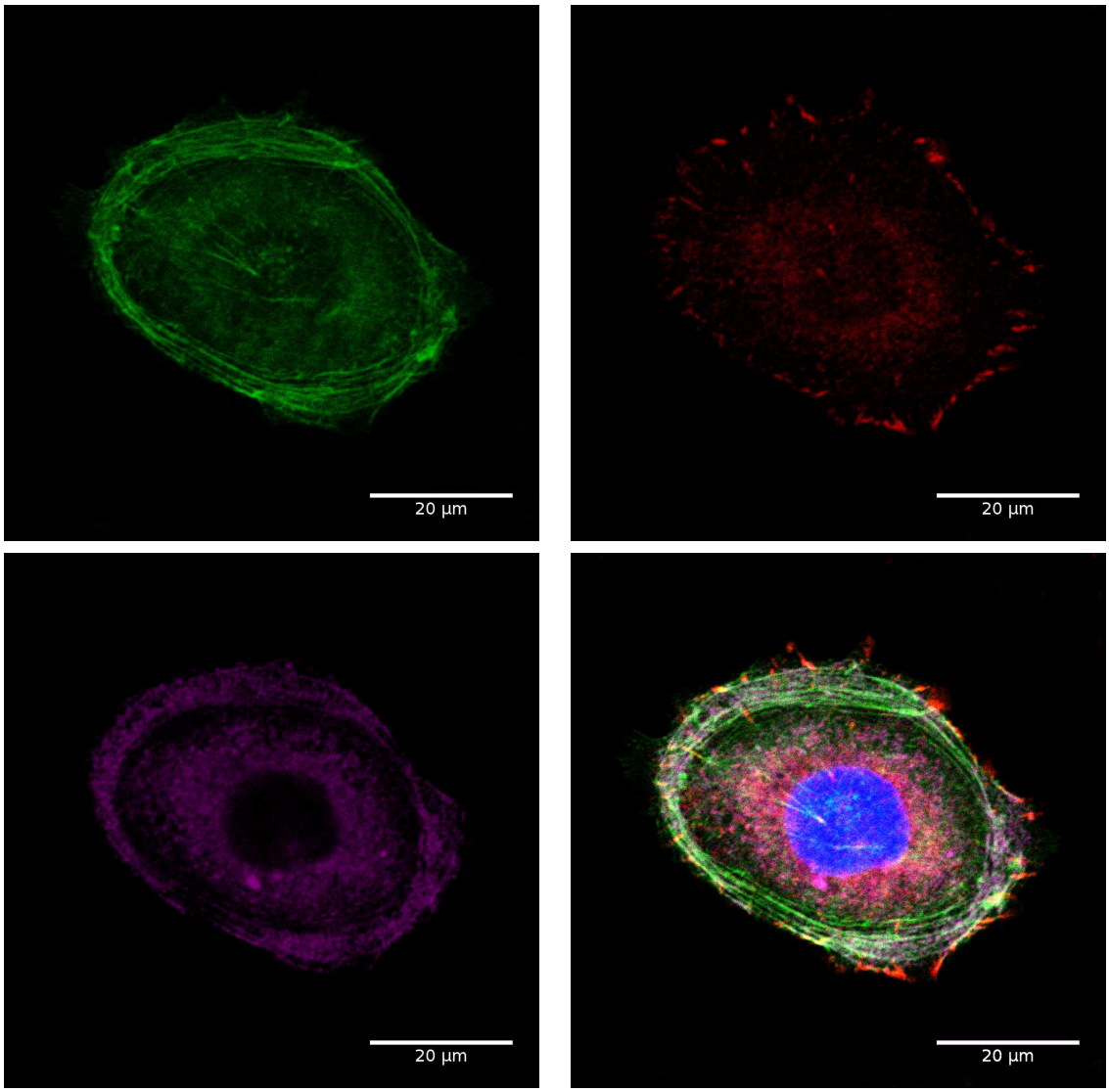

Figure 8: **Fluorescent images of RT112 cancer cells adhering on PA gel.** Gel stiffness is 10kPa). From left to right and top to bottom: cells are stained for actin with Phalloidin Alexa 488 (green), anti–paxillin for focal adhesion sites (red), anti–myosin antibody for myosin IIA (magenta) and Hoechst for nuclei (blue).

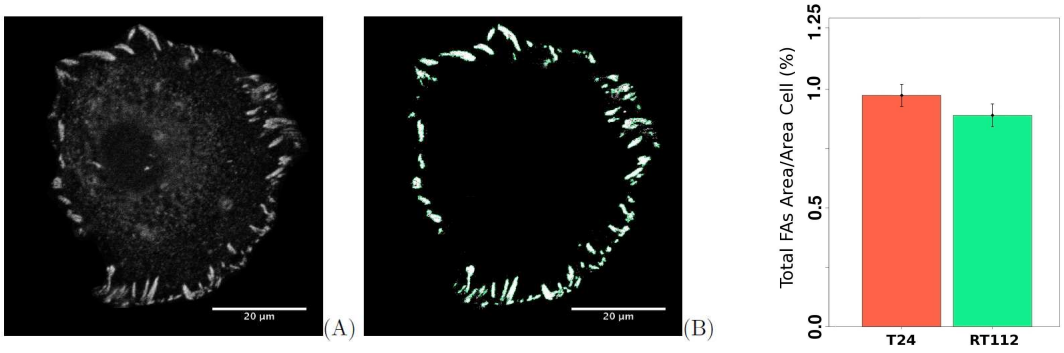

Figure 9: **Focal adhesions. A:** Microscopy image of focal adhesions. **B:** Details of segmentation procedure for focal adhesions calculation. Bar–plot representing total area of focal complexes (>0.5 μm^2) divided by cell area ($p = 0.25$). See also Table 1 for details.

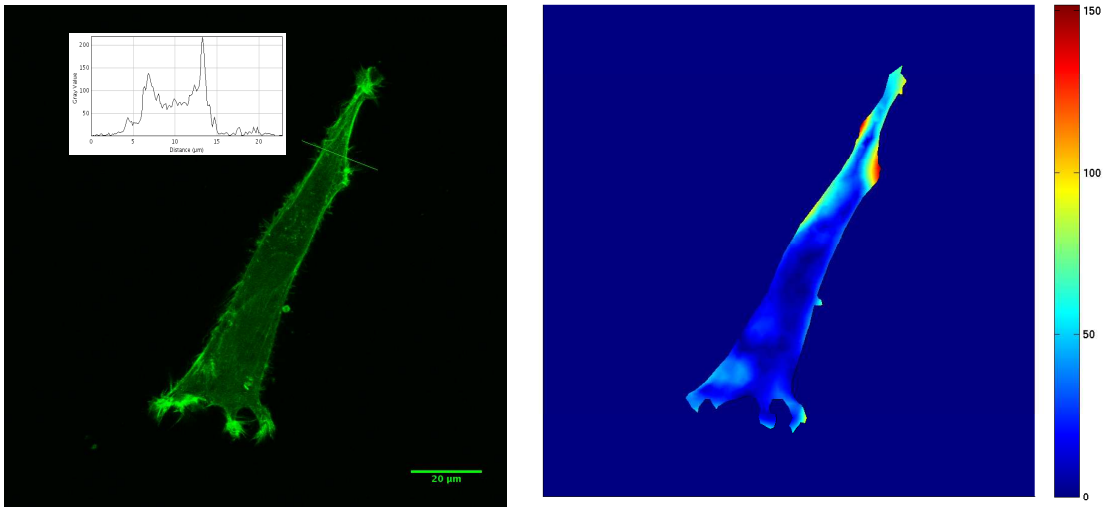

Figure 10: **Image of T24 cancer cell transfected for actin.** PA gel substrate of stiffness 10kPa. Fluorescent image with insert indicating the level of actin expression for the line drawn. Corresponding traction force map (in Pa).

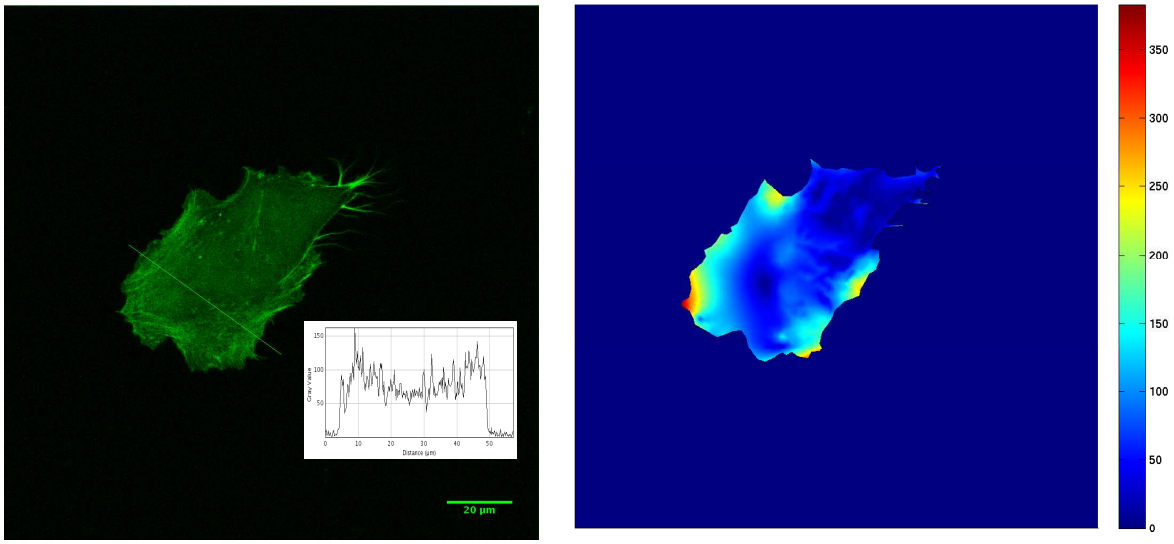

Figure 11: **Image of RT112 cancer cell transfected for actin.** PA gel substrate of stiffness 10kPa. Fluorescent image with insert indicating the level of actin expression for the line drawn. Corresponding traction force map (in Pa).

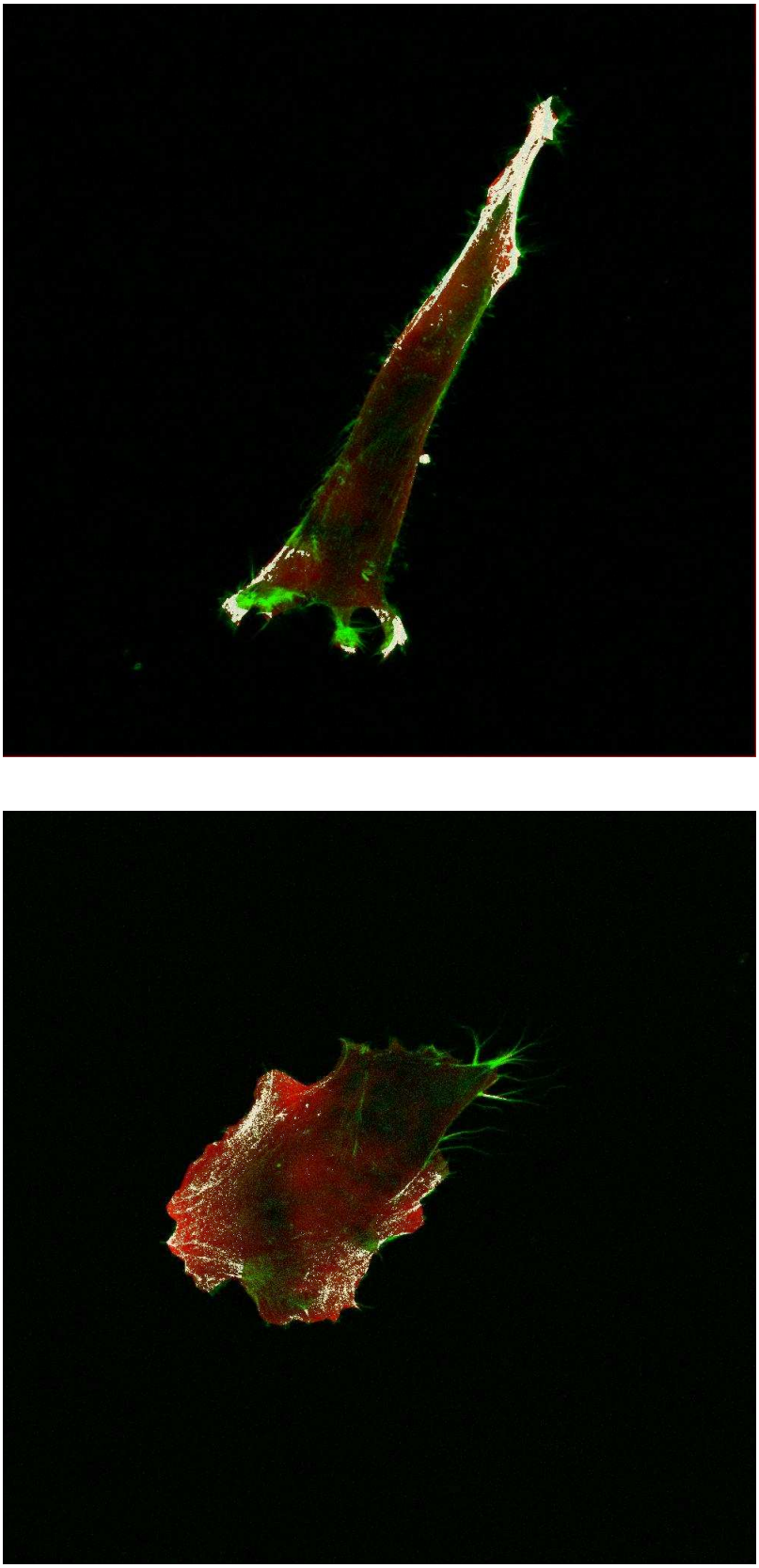

Figure 12: **Colocalization of the actin and force levels.** T24 cell (top) and RT112 cell (below). Larger actin areas are found with the RT112 cell.